Bright correlated four photons from spontaneous four-wave mixing

Yifan Li,[1] Justin Yu Xiang Peh,[1] Chang Hoong Chow,[1] Boon Long Ng,[1] Vindhiya Prakash,[1] and Christian Kurtsiefer[1,2]

[1] *Centre for Quantum Technologies, National University of Singapore, 3 Science Drive 2, Singapore 117543*
[2] *Department of Physics, National University of Singapore, 2 Science Drive 3, Singapore 117551*[*]

..... abstract to come here...

I. INTRODUCTION

Multiphoton states are states with more than two photons entangled or correlated in single or multiple modes. Such states are a fundamental resource for quantum sciences and technologies [1]. At a foundational level, multiphoton GHZ and W states have enabled powerful tests to disprove local realistic theories [2] and explore unique entanglement classes [3, 4] Multiphoton states enable secure communication protocols [5, 6] and also find application in quantum metrology [7]. In the form of cluster states, they are essential for scalable and resource efficient photonic quantum computing [8, 9]. States with four photons have also been used to encode decoherence-resistant quantum information [10].

(Part in Italics to be removed) Several types of entangled multiphoton states, such as three and four-photon GHZ states have been prepared by interfering and combining photon pairs from spontaneous parametric downconversion (SPDC) in independent crystals [1, 2, 11–15]. Another approach utilizes the onset of laser-like stimulation in SPDC, by retro-reflecting a pulsed pump and an initially generated pair to stimulate the generation of further pairs entangled with the reflected two-photon state [16, 17]. However, such schemes require synchronized pump pulsing and complicated geometries for erasure of which-path information. Without the need for such complicated schemes, It is well known that multiphoton states can be directly produced by strong pumping of non-linear processes like SPDC and spontaneous four-wave mixing (SFWM), where the probability of producing more than one photon-pair increases with the pump power [18, 19]. In directly pumping an SPDC process, the probability of producing entangled four photons is twice as high as producing two independent entangled pairs, due to bosonic enhancement [20, 21] Highly entangled W states have also been produced by analyzing the higher-order component in a directly pumped SPDC process [22].

Although there have been theoretical explorations of the rich temporal structure of correlated photon states from SPDC or SFWM [23], direct analysis of the output from SPDC without modification by filtering has been challenging due to the jitter and response averaging of detectors [24]. Correlated photons from SPDC typically have very short coherence lengths, shorter than the length of the SPDC crystal itself. Thus, in the above cases, pulsed pumps with large instantaneous powers and narrowband filters are used to isolate and analyze correlated multiphoton states from the same downconversion event. This leads to losses. The large bandwidth of photons from SPDC also limits their use in memory and repeater schemes that require efficient interfacing with material quantum systems.

Spontaneous four-wave mixing in atomic clouds is an excellent and bright [25**?**] alternative to produce narrowband photons with long coherence times [26–30]. Photons from this process can be spectrally shaped to be narrower or wider than atomic transition linewidths, making them well-suited for quantum networking applications such as memory, repeater, and entanglement distribution schemes involving atoms. Furthermore, their long coherence times, typically in the order of tens of nanoseconds, allow them to be well resolved by off-the-shelf photon detection electronics. Here, we demonstrate that SFWM in a cold atomic cloud is a source for producing time correlated four-photons. The long coherence length of the correlated photon-pairs produced typically exceeds the length of the non-linear medium. This can lead to bosonic enhancement in the collective emission of a correlated second pair within the coherence time of one pair Thus, it is possible to observe a correlation within higher-order pair generation in direct continuous-wave (cw) pumping at nominal powers without the need for filters.

In cw-pumped SFWM within an atomic medium, the third-order nonlinear interaction of a weak narrowband *pump* laser and *coupling* laser with the medium generates narrowband, correlated optical fields which we call Stokes and anti-Stokes by convention. A single frequency conversion process produces the following state that can contain multiple Stokes and anti-Stokes photons [31–33],

$$|\Psi\rangle = \frac{1}{\beta}\sum_{n=0}^{\infty}(\alpha)^n\,|n,n\rangle \tag{1}$$

Here, $\beta \equiv \cosh\zeta$, $\alpha \equiv \tanh\zeta$, ζ is related to the effective interaction Hamiltonian and is proportional to the pump power, and $|n,n\rangle$ indicates correlated Fock states with n photons each in the Stokes and anti-Stokes modes. A complete expression for the interaction Hamiltonian and the nonlinear susceptibilities can be found in [27, 34]. From Eq. 1, it is evident that

[*] christian.kurtsiefer@gmail.com

at small interaction strengths ($\zeta \approx 0$) the probability of generating states with four photons relates to the probability of producing pairs as $P_4 = P_2^2$. In this case the four photon states contain correlated and entangled quadruplets of two Stokes and anti-Stokes photons generated within a single SFWM process[35]. However, in the event of multiple independent frequency conversion processes occurring, four-photon states can contain uncorrelated and unentangled double pairs. In this case, the probability of creating n pairs (P_n) within a certain time window, is described by a Poisson distribution of mean u, $P_n = e^{-\mu}\mu^n/n!$. For small μ, $P_4 \approx P_2^2/2$.[35].

Here, we study the four photon component from SFWM in a cold cloud of Rb^{87} atoms using double Hanbury Brown and Twiss (HBT) type setups, one in each of the correlated modes. We introduce an efficient technique for identifying coincidences across multiple detectors, which helps us analyze three-fold and four-fold coincidences of the photons generated from the nonlinear interaction. The generation rate for quadruplets scales quadratically with the pump power as compared with the generation of pairs, which scales linearly. We analyze the temporal structure of the detected coincidences and identify a strong contribution of correlated four-photons or quadruplets over uncorrelated but accidental double-pairs. Within a correlation window of 20 ns we observe a peak in three-fold coincidences that is twice the value at longer delays. This indicates that we observe quadruplets correlated in time within 20 ns, as opposed to a Poisson distribution of uncorrelated four photons detected outside the correlation time. This confirms the presence of stimulation or bosonic enhancement in the generation of the second-pair within the correlation time [16, 35], and that the entire macroscopic ensemble of individual atoms behaves coherently as a unit in the generation of quadruplets. Having taken into account channel losses and detector efficiencies, we estimate an instantaneous photon quadruplet generation rate of 2.3×10^6 counts per second close to saturation of the nonlinear frequency conversion.

Multiphoton narrowband photons have so far been demonstrated by spatially multiplexing two SFWM events, spontaneous Raman events, and cascaded geometries [36–39]. Our results show that direct pumping holds potential to be a simpler alternative to producing multiphotons with the possibility of being entangled. To our knowledge, microscopic and macroscopic phenomenological models of SFWM as a collective process involving individual atomic emitters have dealt only with the generation of photon-pairs [40, 41]. Our results pave the way for the extension of such models to better understand the microscopic origin of correlated multiphoton states.

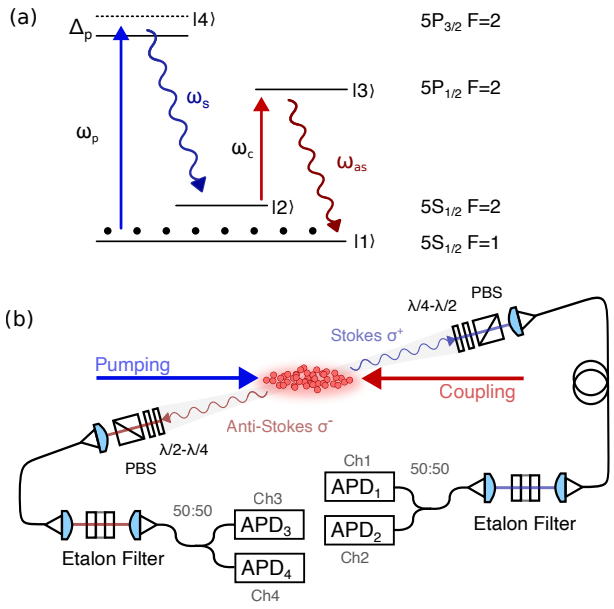

FIG. 1. (a) Energy levels involved in the Double-Λ spontaneous four-wave mixing in ^{87}Rb. Solid blue and red arrows indicate cw pump and coupling fields respectively. Wiggly blue and red arrows indicate generated Stokes and anti-Stokes fields. Black dots indicate initialization of atoms in the $F = 1$ hyperfine ground state. (b) Schematic of experimental setup. The pumping and coupling beams have a waist of ~ 0.85 mm. The collection spatial mode is focused on the atomic ensemble with a waist of 175 μm. Channels 1 and 2 analyze the Stokes field, and Channels 3 and 4 the anti-Stokes fields in a Hanbury-Brown-Twiss like setup. $\lambda/2$: Half waveplate, $\lambda/4$: quarter waveplate, PBS: polarising beamsplitter, Ch: channel, APD: avalanche photodiode.

II. EXPERIMENTAL SETUP

Our scheme is based on SFWM using a double-Λ configuration of energy levels in a cold cloud of ^{87}Rb atoms, similar to the systems reported in [28, 42]. The SFWM process is driven by a weak cw pump (of frequency ω_p) detuned by Δ_p from $|5S_{1/2}, F = 1\rangle \rightarrow |5P_{3/2}, F = 2\rangle$ and a strong cw coupling laser (of frequency ω_c) resonant to the $|5S_{1/2}, F = 2\rangle \rightarrow |5P_{1/2}, F = 2\rangle$ transition. The Stokes photons are generated at a frequency ω_s close to the $|5P_{3/2}, F = 2\rangle \rightarrow |5S_{1/2}, F = 2\rangle$ transition and the anti-Stokes photons have a frequency ω_{as} resonant to the $|5P_{1/2}, F = 2\rangle \rightarrow |5S_{1/2}, F = 1\rangle$ transition (refer Fig.1(a)). The fields are circularly polarized, orthogonal to each other, and are directed at an elongated magneto-optical trap (MOT) of cold ^{87}Rb atoms, along the long axis in a counter-propagating configuration (Fig.1 (b)). The SFWM process is precluded by initializing atoms in the MOT to the $|5S_{1/2}, F = 1\rangle$ hyperfine ground state via optical pumping. The MOT trapping beams are switched off during the SFWM measurement. The

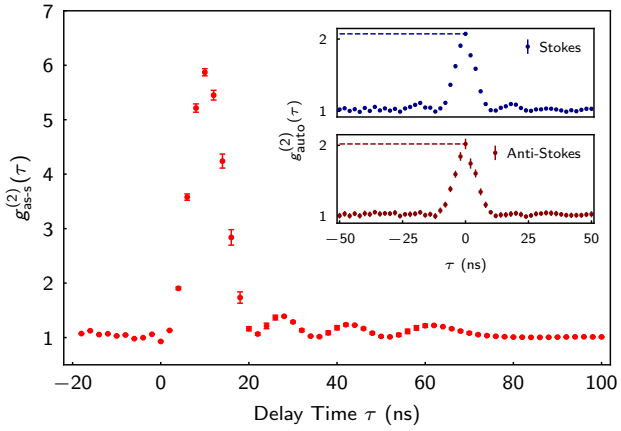

FIG. 2. Normalized second-order correlation. (a) The Stokes-anti-Stokes cross-correlation as a histogram of coincidences for various delays τ, normalized by the Stokes and anti-Stokes singles rates for a 2 ns bin size and an integration time of 150 s. Results averaged over 17 measurements. Oscillations of periodicity 18 ns are caused by the Rabi frequency of the coupling field. Insets: Unheralded autocorrelation measurements of Stokes photons $g^{(2)}_{s,s}(\tau)$ (blue) and anti-Stokes photons $g^{(2)}_{as,as}(\tau)$ (red) (jointly labeled $g^{(2)}_{\text{auto}}(\tau)$).

optical depth (OD) of the atomic cloud is $\sim$ 30. The spatial modes for collection the Stokes and anti-Stokes photons are focused on the atomic ensemble with a waist of 175 μm. The collection modes are at an angle of 1° to the pump and coupling fields, to reduce background scattering. Polarization filters and temperature controlled etalon filters (bandwidth $\sim$ 100 MHz) are implemented in both Stokes and anti-Stokes collection arms to suppress unwanted photons. The photons collected in the Stokes and anti-Stokes arms are split using 50:50 fiber beamsplitters (BS) and detected using avalanche photodiodes (APDs). A timestamp card with 2 ns timing resolution records the photon arrival times in each of these four channels. Second, third and fourth-order field correlations are analyzed using this data.

III. RESULTS

A. Second-Order Correlation

We measure the second-order intensity correlations as a first step towards characterizing the statistical properties of the generated fields. The normalized second-order correlation between stationary fields $\hat{E}_i$ in mode i, detected at time t_i, and $\hat{E}_j$ detected at time $t_j = t_i + \tau_{ji}$ is [43]

$$g^{(2)}_{ji}(\tau_{ji}) = \frac{\langle \hat{E}^\dagger_i(t_i)\hat{E}^\dagger_j(t_i+\tau_{ji})\hat{E}_j(t_i+\tau_{ji})\hat{E}_i(t_i)\rangle}{\langle \hat{E}^\dagger_j(t_i+\tau_{ji})\hat{E}_j(t_i+\tau_{ji})\rangle\langle \hat{E}^\dagger_i(t_i)\hat{E}_i(t_i)\rangle}\,, \tag{2}$$

where $i,j \in \{s, as\}$ for the Stokes (s) and anti-Stokes (as) modes.

The second-order autocorrelations $g^{(2)}_{s,s}(\tau)$, $g^{(2)}_{as,as}(\tau)$ and cross-correlation $g^{(2)}_{s,as}(\tau)$ were measured for pump and coupling powers of about 800 μW and 10 mW respectively and a pump detuning of $\Delta_p = 40$ MHz. From the $g^{(2)}_{s,as}(\tau)$ results shown in Fig.2 we infer a correlation time of around $\Delta t = 16$ ns between the Stokes and anti-Stokes photons. The oscillations in the coincidences are due to the strong coupling beam which leads to an oscillation of population between energy levels $|2\rangle$ and $|3\rangle$ at an effective Rabi frequency of $2\pi \times 55\,\text{MHz}$[28]. The pair generation rates inferred from these measurements are given in section III E.

The Stokes and anti-Stokes modes independently display thermal statistics as seen from their intensity autocorrelation at $\tau = 0$ (inset in Fig.2). We measure $g^{(2)}_{s,s}(0) = 2.07 \pm 0.02$ for the Stokes mode and $g^{(2)}_{as,as}(0) = 2.02 \pm 0.07$ for the anti-Stokes mode.

B. Triple Coincidences

We analyze the temporal distribution of coincidences involving more than two detections, to determine the ratio of correlated double-pairs to two independent pairs detected together by chance. Both these scenarios lead to states containing multiples of Stokes-anti-Stokes pairs and there is no physical mechanism that generates states involving three photons. Thus, a measurement of triplet coincidences involving two Stokes and one anti-Stokes photons or two anti-Stokes and one Stokes photon provides similar information to a four-fold coincidence measurement of two anti-Stokes and two Stokes photons, while being simpler to acquire and visualize.

The normalized third-order correlation between the Stokes and anti-Stokes modes from two anti-Stokes detections at times t_3 and t_4 and a Stokes detection at time t_s is

$$g^{(3)}_{as,as,s}(t_3,t_4,t_s) = \frac{\langle \hat{E}^\dagger_s(t_s)\hat{E}^\dagger_{as}(t_3)\hat{E}^\dagger_{as}(t_4)\hat{E}_{as}(t_4)\hat{E}_{as}(t_3)\hat{E}_s(t_s)\rangle}{\langle \hat{E}^\dagger_s(t_s)\hat{E}_s(t_s)\rangle\langle \hat{E}^\dagger_{as}(t_3)\hat{E}_{as}(t_3)\rangle\langle \hat{E}^\dagger_{as}(t_4)\hat{E}_{as}(t_4)\rangle} \tag{3}$$

where the numerator gives the triple-coincidence rate $G^{(3)}_{as,as,s}(t_3,t_4,t_s)$. This can be expressed in terms of second-order correlations as shown in Eq.A7.

Fig.3 shows $g^{(3)}_{as,as,s}$ for triplets from an anti-Stokes detection each in channels 3 (at t_3) and 4 (at t_4) and a Stokes detection in either of channels 2 or 1 (at t_s), where the measurement was performed for the same conditions

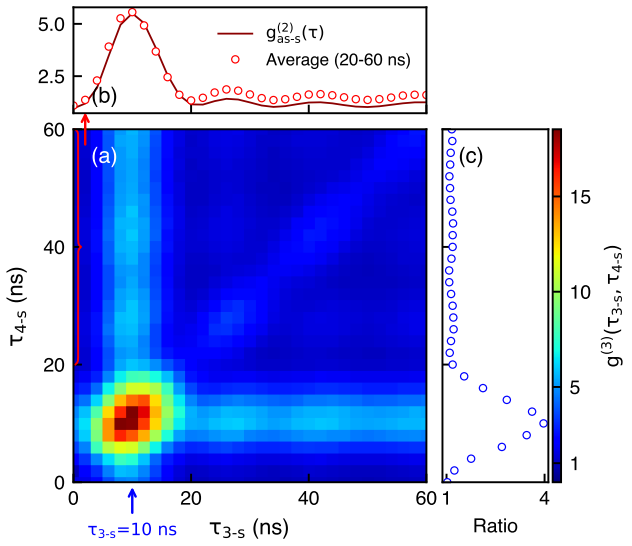

FIG. 3. Normalized third-order correlation. (a) Normalized triple coincidences $g^{(3)}_{as,as,s}$ for various delays τ_{3s} and τ_{4s} between a detection in Ch3 and Ch4 respectively and a heralding Stokes photon in either of Ch1 or Ch2. Coincidences analyzed from data acquired over a measurement duration T_m of 0.7 h, normalized by the accidental triplet rate $R_sR_3R_4\delta t^2T_m$, where the time bin $\delta t = 2$ ns and R_i is the singles count in channel i. The $g^{(3)}_{as,as,s}$ peak value of 18 indicates strongly correlated triplets. (b) Comparison of the vertical ridge with $g^{(2)}_{as,s}$. Red dots: Mean normalized triplet count, averaged over τ_{4s} from 20 ns to 60 ns. Solid line: normalized cross-correlation function $g^{(2)}_{as,s}(\tau_{3s})$ between Stokes and Ch3. (c) Ratio of normalized triple coincidence peak value with the average value along the vertical ridge away from the peak. Blue dots: Triple coincidences at $\tau_{3s} = 8$ ns divided by mean triple coincidences at $\tau_{3s} = 8$ ns and $\tau_{4s} = 20 - 60$ ns. The peak is approximately 4 times the value in the ridge.

as in section III A. The results are represented in terms of relative delays $\tau_{3s} = t_3 - t_s$ and $\tau_{4s} = t_4 - t_s$. The technique used to identify triplets from pair coincidences is described in the Appendix B.

The features in Fig. 3 can be intuitively understood by analyzing Eq.A7 over various delays. For a coherence time Δt for the Stokes and anti-Stokes photons, when $\tau_{3s}, \tau_{4s}, \tau_{34} \gg \Delta t$, the triplet rate reduces to the background accidental rate $R^3(0)$ which is normalized to 1 here. When $\tau_{3s}, \tau_{4s}, \gg \Delta t$ and $\tau_{34} \lesssim \Delta t$, the autocorrelation in the anti-Stokes mode dominates the result ($g^{(3)}_{as,as,s}(\tau_{3s}, \tau_{4s}, \tau_{34}) \rightarrow g^{(2)}_{as,as}(\tau_{34})$). In this case, the triplets are caused by the combination of an accidental click in the Stokes mode with a bunched thermal state in the anti-Stoked mode, forming the moderately bright diagonal in Fig. 3.

For $\tau_{3s}, \tau_{34} \gg \Delta t$ but $\tau_{4s} \lesssim \Delta t$ (horizontal ridge) or when $\tau_{4s}, \tau_{34} \gg \Delta t$ but $\tau_{3s} \lesssim \Delta t$ (vertical ridge) the cross-correlation between anti-Stokes (in Ch4 or Ch3 respectively) and Stokes photon-pairs are the dominant contributions. Here, the triplets are formed by a combination of a correlated Stokes-anti-Stokes pair with an uncorrelated photon in the other anti-Stokes channel. Thus, the maximum mean value in the horizontal and vertical ridges is equal to $g^{(2)}_{s,as}(0)$ as seen in Fig. 3 (b).

In the region where $\tau_{3s}, \tau_{34}, \tau_{4s} \lesssim \Delta t$ the coincidences increase several-fold. From Eq.A7, using $g^{(2)}_{as,as}(0) = 2$, the theoretical peak value of the normalized triplet rate is $g^{(3)}_{as,as,s}(0,0,0) = 4g^{(2)}_{as,s}(0) - 2 \approx 4g^{(2)}_{as,s}(0)$ when $g^{(2)}_{as,s}(0) \gg 1$, a condition true for highly non-classical pair sources. Thus, theoretically the peak is 4 times the maximum in either of the horizontal or vertical ridges when the output contains highly correlated four-photon states. When the output contains fewer correlated four-photons and more uncorrelated double-pairs from multiple SFWM events, the triplet peak at zero delays would arise from the overlapping of the ridges and would be closer to 2 times the maximum in either of the horizontal or vertical ridges.

Due to the long coherence time of the Stokes and anti-Stokes photons, our triplet measurement is not limited by averaging effects due to detector resolution, which would have otherwise reduced the maximum of the triple-coincidence peak. We see from Fig.3 (c) that in our measurement, the $g^{(3)}_{as,as,s}$ peak is 18 and is about four times the mean along the vertical ridge (outside the central 20 ns window). Thus, we verify that the output of the SFWM process contains strongly correlated double-pairs, that contribute to the high three-fold coincidences in the triplet measurement.

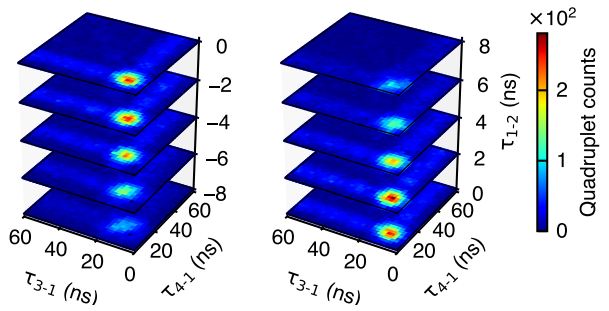

FIG. 4. Quadruple-coincidence detection. Each slice shows unnormalised four-fold coincidences from a detection in each of Ch1 to Ch4 for a fixed delay τ_{12} with a 2 ns time bin, and a range of delays τ_{31} and τ_{41}. Data acquired over a measurement duration of 0.7 hr. The coincidences are peaked for $\tau_{12} = 0 \pm 2$ ns and τ_{31} and $\tau_{41} = 8 \pm 2$ ns.

C. Quadruple coincidences

We search for four-fold coincidences between detections of two photons in the anti-Stokes mode and two photons in the Stokes mode to obtain the

double-pair generation rate and to directly verify the generation of correlated double-pairs from our SFWM source. The quadruplet rate for four-fold coincidences from two Stokes detections at times t_1 and t_2 respectively and two anti-Stokes detections at time t_3 and t_4 respectively is described by the correlation function

$$G^{(4)}_{s,s,as,as}(t_1,t_2,t_3,t_4) = \langle \hat{E}^\dagger_{as}(t_4)\hat{E}^\dagger_{as}(t_3)\hat{E}^\dagger_{s}(t_2)\hat{E}^\dagger_{s}(t_1)\hat{E}_{s}(t_1)\hat{E}_{s}(t_2)\hat{E}_{as}(t_3)\hat{E}_{as}(t_4)\rangle. \quad (4)$$

The normalized fourth-order cross-correlation is

$$g^{(4)}_{s,s,as,as}(t_1,t_2,t_3,t_4) = \frac{\langle \hat{E}^\dagger_{as}(t_4)\hat{E}^\dagger_{as}(t_3)\hat{E}^\dagger_{s}(t_2)\hat{E}^\dagger_{s}(t_1)\hat{E}_{s}(t_1)\hat{E}_{s}(t_2)\hat{E}_{as}(t_3)\hat{E}_{as}(t_4)\rangle}{\langle \hat{E}^\dagger_{s}(t_1)\hat{E}_{s}(t_1)\rangle\langle \hat{E}^\dagger_{s}(t_2)\hat{E}_{s}(t_2)\rangle\langle \hat{E}^\dagger_{as}(t_3)\hat{E}_{as}(t_3)\rangle\langle \hat{E}^\dagger_{as}(t_4)\hat{E}_{as}(t_4)\rangle}. \quad (5)$$

$G^{(4)}_{s,s,as,as}(t_1,t_2,t_3,t_4)$ can be expressed in terms of the first-order auto and cross-correlations between the modes as shown in Appendix A.

We search for four-fold coincidences for detections at times t_1 to t_4 in channels 1 to 4, under the same conditions as in section III A, within a window of 100 ns. We represent the data as sliced density plots where each slice shows quadruplets for a fixed delay τ_{12} and various relative delays τ_{31} and τ_{41}. We see the maximum density of quadruplets clustered around $\tau_{12} = 0 \pm 2$ ns and τ_{31} and $\tau_{41} = 8 \pm 2$ ns. Outside a 20 ns window centered at $(\tau_{12}, \tau_{31}, \tau_{41}) = (0\,\text{ns}, 8\,\text{ns}, 8\,\text{ns})$ the quadruplet count drops significantly to the background level indicating the presence of highly-correlated quadruplets within 20 ns. Every slice contains bright horizontal and vertical ridges from four-fold coincidences between accidentals and a correlated pair between Ch4-Ch1 or Ch3-Ch1 respectively. A relatively dull diagonal due to four-fold coincidences between accidentals and thermally bunched photons in Ch3-Ch4 can also be seen.

D. Detection Rates

From the data, we obtain singles rates in each channel (R_i, $i \in \{1,2,3,4\}$) and singles in the Stokes (anti-Stokes) modes as $R_{s(as)} = R_{1(3)} + R_{2(4)}$. From the pair, triplet and quadruplet coincidence measurements we obtain the measured pair rate as $R_p = R_{13} + R_{14} + R_{23} + R_{24}$ (R_{ij} is the rate for coincidences between channels i and j), triplet rate $R_t = R_{134} + R_{234} + R_{123} + R_{124}$ (R_{ijk} is the rate for coincidences between channels i, j and k), and quadruplet rate (R_q) defined within a $t_c = 20$ ns coincidence window, without subtraction of accidentals. t_c of 20 ns is appropriate as the detection of correlated double-pairs is peaked within this window as seen from sections III B and III C. Fig.5 shows the singles, pairs, triplets and quadruplet rates as functions of pump power. The production of photon pairs and quadruplets saturates at pump powers over a mW. At

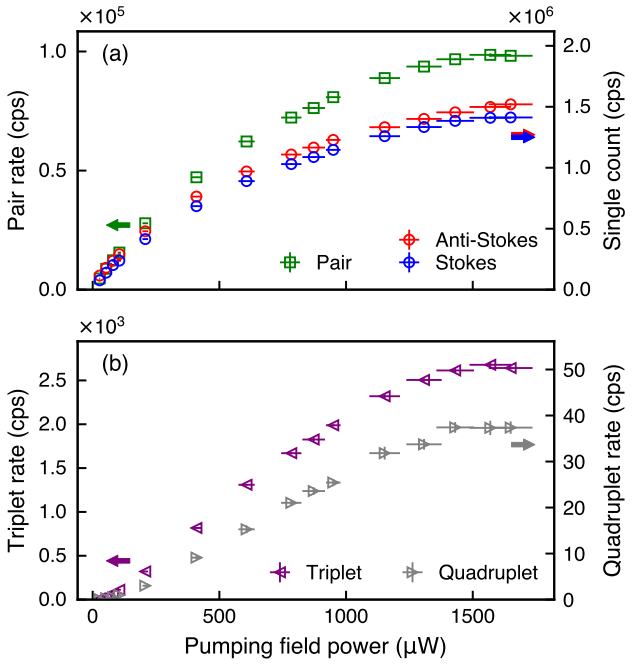

FIG. 5. Detection rates as a function of pump power (a) Single count rates (left axis) in Stokes (blue dots) and anti-Stokes channels (red dots) and correlated photon pair rate (green dots, right axis) as functions of pumping field power. (b) Correlated photon triplet rates across three detector channels (magenta dots, left axis) and correlated photon quadruplet rate (grey dots, right axis) as functions of pumping field power. The detuning of the pumping field is 40 MHz, while the coupling field is resonant with a fixed power of 10 mW. The atomic cloud has OD $\simeq$ 30.

low pump powers (approximately < 200 μW) the pair rate scales linearly with the pump power while the triplet and quadruplet rate scales quadratically with the pump power.

This is better visualized in Fig.6, where the pair, triplet and quadruplet rates are shown relative to singles rates in the Stokes and anti-Stokes modes, with axes in log scale. R_p scales approximately linearly with R_s and R_{as}, with fitted slope parameters of 0.86 ± 0.02 and 0.95 ± 0.03, respectively. The slopes of R_t and R_q relative to R_s are 1.87 ± 0.02 and 2.11 ± 0.03, respectively, while the slopes of R_t and R_q relative to R_{as} are found to be 1.97 ± 0.04 and 2.34 ± 0.03, respectively. The slopes of R_t and R_q are both close to 2 which is expected from the fact that triplet and quadruplet photons originate from the same physical processes. Furthermore, these measurements indicate that the rate at which double-pairs are detected scales close to quadratically with the rate of detecting correlated photon-pairs, which shows that the photons in the double-pairs are produced from a higher-order process in frequency conversion. However, we note that for a more accurate relationship between the probability of generating states with four photons

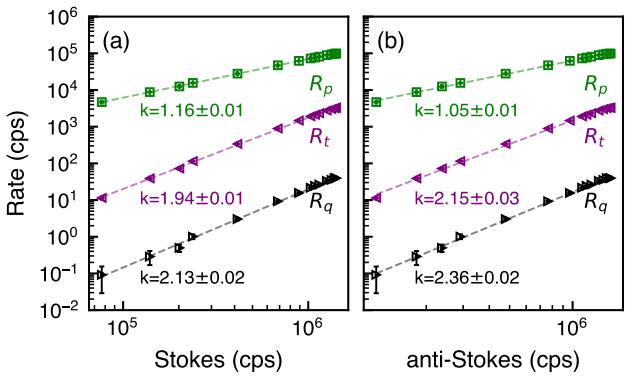

FIG. 6. Ratio of pairs, triplets and quadruplets to singles. The photon pair rate R_p (green dots), photon triplet rate R_t (magenta dots), and photon quadruplet rate R_q (black dots) from Fig. 5 represented in log-scale relative to the singles count rate R_s in Stokes mode (a) and singles count rate the anti-Stokes R_{as} (b). Both axes are plotted on a logarithmic scale. The variation in the single count rates is achieved by varying the pump power while keeping all other parameters constant.

and states with pairs of photons, we need to correct for accidentals and factor losses from inefficient optical paths, photon collection and detection in each channel.

E. Accidental corrected detection rates and generation rate

At fixed pump and coupling powers of 800 μW and 10 mW respectively, and $\Delta_p = 40$ MHz, the mean value of singles rates R_s is $(1.04\pm0.07)\times10^6$ cps and R_{as} is $(1.10\pm0.06)\times10^6$ cps. To determine the rates of truly correlated pairs, triplets and quadruplets from the detected pair, triplet, and quadruplet rates, we performed accidental correction as described in the Appendix E. This gives a correlated pair detection rate $c_p = (4.8 \pm 0.3) \times 10^4$ cps.

As we can see in Appendix E, the correction of accidentals for triplets depends on which mode is used as the herald. Thus, we report channel-specific accidental-corrected triplet rates. The corrected rate of detected photon triplets consisting of one Stokes photon and one anti-Stokes photon each in Ch3 and Ch4 is $c_{134} + c_{234} = (251 \pm 10)$ cps, while the rate for triplets consisting of a Stokes photon each in Ch1 and Ch2 and one anti-Stokes photon is $c_{123} + c_{124} = (246 \pm 7)$ cps. Here c_{ijk} is the rate of correlated triplets between channels i, j and k. The correlated photon quadruplet rate after accidental-subtraction, for a detection in each of the four channels, is found to be $c_q = (2.9 \pm 0.4)$ cps. The total transmission and detection probability in each channel $k \in \{1, 2, 3, 4\}$, which includes transmission of the collection and filtering setup, splitting efficiency of the fiber-based 50:50 beamsplitter and quantum efficiency of the detector in the respective channel is denoted by η_k. Following the procedure in Appendix C to estimate the losses in each channel, we find the total efficiencies to be $\eta_1 = 0.022$ and $\eta_2 = 0.023$ for channels 1 and 2 pertaining to the Stokes modes, and $\eta_3 = 0.025$ and $\eta_4 = 0.021$ for channels 3 and 4 of the anti-Stokes mode.

We infer the generation rates of pairs g_p and double-pairs g_q from detected accidental-corrected rates of pairs, triplets and quadruplets by factoring in the channel losses as described in D. Based on this, we report a double-pair generation rate of $g_q = 2.5(4) \times 10^6$ cps and a pair generation rate of $g_p = 1.3(3) \times 10^7$ cps at a pump power of 800 μW.

IV. CONCLUSION

•

Appendix A: Double, Triple and Quadruple Coincidences

Here we express the double, triple and quadruple coincidence rates in terms of the phase sensitive first-order cross-correlation,

$$C(\tau_{ij}) = \langle \hat{E}_i(t+\tau_{ij})\hat{E}_j(t)\rangle \tag{A1}$$

and the first-order autocorrelation

$$R(\tau_{ij}) = \langle \hat{E}_i^\dagger(t+\tau_{ij})\hat{E}_j(t)\rangle \tag{A2}$$

where $\{i, j\} \in \{s, as\}$ to represent the Stokes or anti-stokes modes or $\{i, j\} \in \{1, 2, 3, 4\}$ to represent one of the four detection channels. Note, $R(0)$ is the pair generation rate.

It is well known that when the state under consideration is the output of a parametric photon-pair production such as SPDC or SFWM, the Gaussian moment factoring theorem can be applied to the intensity correlations in Eq.2 to give the following expression for the normalized intensity cross-correlation [44]

$$g^{(2)}_{s,as}(\tau) = 1 + \frac{|C(\tau_{s,as})|^2}{|R(0)|^2}, \tag{A3}$$

and the normalized intensity autocorrelation as

$$g^{(2)}_{i,i}(\tau) = 1 + \frac{|R(\tau_{i,i})|^2}{|R(0)|^2} \tag{A4}$$

The triple-coincidence rate $G^{(3)}_{as,as,s}$ for two anti-Stokes detections and a single Stokes detection,

$$G^{(3)}_{as,as,s}(t_3,t_4,t_s) = \langle \hat{E}_s^\dagger(t_s)\hat{E}_{as}^\dagger(t_3)\hat{E}_{as}^\dagger(t_4)\hat{E}_{as}(t_4)\hat{E}_{as}(t_3)\hat{E}_s(t_s)\rangle \tag{A5}$$

can be similarly expanded and expressed in terms of relative delays to give [23, 24]

$$\begin{aligned}G^{(3)}_{as,as,s}(\tau_{3s},\tau_{4s},\tau_{34}) =& R(0)[R(0)^2+|R(\tau_{34})|^2]\\ &+R(0)[|C(\tau_{3s})|^2+|C(\tau_{4s})|^2]\\ &+2\mathrm{Re}\{C(\tau_{3s})C^*(\tau_{4s})R(\tau_{34})\}.\\ =& R(0)^3 g^{(2)}_{as,as}(\tau_{34})+R(0)^3 g^{(2)}_{as,s}(\tau_{3s})\\ &+R(0)^3 g^{(2)}_{as,s}(\tau_{4s})-2R(0)^3\\ &+2R(0)^3\sqrt{g^{(2)}_{as,s}(\tau_{3s})-1}\\ &\sqrt{g^{(2)}_{as,s}(\tau_{4s})-1}\times\sqrt{g^{(2)}_{as,as}(\tau_{34})-1}.\end{aligned} \tag{A6}$$

This equation shows that accidental triplet events are a sum of four contributions: accidental singles detected in each of the three channels, a correlated pair between the Stokes mode and Ch3 (Ch4) with an accidental in Ch4 (Ch3) and thermally bunched photons in the anti-Stokes (causing coincidences in Ch3 and Ch4) with an accidental single in the Stokes mode (Ch1 or Ch2). The normalized third-order correlation can be expressed in terms of the normalized intensity auto and cross correlations using A4 and A3 as

$$\begin{aligned}g^{(3)}_{as,as,s}(\tau_{3s},\tau_{4s},\tau_{34}) =& \frac{G^{(3)}_{as,as,s}(\tau_{3s},\tau_{4s},\tau_{34})}{R(0)^3}\\ =& g^{(2)}_{as,as}(\tau_{34})+g^{(2)}_{as,s}(\tau_{3s})\\ &+g^{(2)}_{as,s}(\tau_{4s})-2\\ &+2\sqrt{g^{(2)}_{as,s}(\tau_{3s})-1}\sqrt{g^{(2)}_{as,s}(\tau_{4s})-1}\\ &\times\sqrt{g^{(2)}_{as,as}(\tau_{34})-1}.\end{aligned} \tag{A7}$$

Similarly, the quadruplet rate for detecting two Stokes photons at times t_1, and t_2 and two anti-Stokes photons at times t_3 and t_4 is given in Eq.A8, where the moment factoring theorem was applied to obtain the following expression in terms of relative delays.

$$\begin{aligned}G^{(4)}_{s,s,as,as}(\tau_{34},\tau_{24},&\tau_{14},\tau_{23},\tau_{21},\tau_{13}) = R(0)^4\\ &+R(0)^2[|R(\tau_{43})|^2+|R(\tau_{21})|^2]\\ &+R(0)^2[|C(\tau_{23})|^2+|C(\tau_{24})|^2]\\ &+R(0)^2[|C(\tau_{13})|^2+|C(\tau_{14})|^2]\\ &+2R(0)\mathrm{Re}\{R(\tau_{34})C^*(\tau_{24})C(\tau_{23})\}\\ &+2R(0)\mathrm{Re}\{R(\tau_{34})C^*(\tau_{14})C(\tau_{13})\}\\ &+2R(0)\mathrm{Re}\{R(\tau_{21})C^*(\tau_{14})C(\tau_{24})\}\\ &+2R(0)\mathrm{Re}\{R(\tau_{21})C^*(\tau_{13})C(\tau_{23})\}\\ &+|R(\tau_{43})|^2|R(\tau_{21})|^2\\ &+|C(\tau_{13})|^2|C(\tau_{24})|^2+|C(\tau_{14})|^2|C(\tau_{23})|^2\\ &+2\mathrm{Re}\{C^*(\tau_{24})C^*(\tau_{13})C(\tau_{14})C(\tau_{23})\}]\\ &+2\mathrm{Re}\{R(\tau_{34})R(\tau_{12})C^*(\tau_{24})C(\tau_{13})\}\\ &+2\mathrm{Re}\{R(\tau_{34})R(\tau_{21})C(\tau_{23})C^*(\tau_{14})\}\end{aligned} \tag{A8}$$

From the 17 terms that sum up to give Q in Eq A8, all terms other than the last three are contributions due to accidentals. Terms 2-7, are due to two accidentals combined with either a correlated Stokes-anti-Stokes pair or bunched photons in one of the Stokes or anti-Stokes modes. Terms 8-11 are caused by an accidental combined with a correlated triplet in three channels. Term 12 is from bunching in both the Stokes and anti-Stokes modes. Terms 13 and 14 are correlated pairs from separate SFWM events contributing to four-fold coincidences. Terms 15, 16 and 17 are due to correlated double-pairs from the same SFWM event.

Appendix B: Event searching algorithms

The search for multiple coincidences over timestamp data of four channels is a computationally resource intensive task. We employ the following strategy to simplify the search. We first identify pair coincidences at various relative delays for each pair from the following possible pairs of Stokes-anti-Stokes channels 1-3, 1-4, 2-3 and 2-4. The triplet coincidences are then identified based on the pair detections that share a photon arrival timestamp. Quadruplet events are identified from triplet detections that share a common timestamp with a pair detection.

For example, to identify triplet events involving Ch1, Ch3, and Ch4, we compare the timestamps of pairs between Ch1 and Ch3 detected at timestamps t_1 and t_3 with pairs between Ch1 and Ch4 detected at timestamps t_1' and t_4. Pair events that share a common timestamp in Ch1 i.e. $t_1 = t_1'$, are taken to form the triplet event (t_1, t_3, t_4). This information can be used to identify quadruplets between the four channels. For this we compare pair events between Ch2 (at t_2) and Ch4 (at time t_4^*) with the previously identified triplet event with times t_1, t_3, t_4. When $t_4 = t_4^*$, the events are combined

to form a quadruplet detection with the timestamp t_1, t_2, t_3, t_4. Thus, we can efficiently search for pair, triplet, and quadruplet events from timestamp data and plot the temporal distribution of these coincidences.

Appendix C: Channel Losses

We characterize the losses in each channel to estimate the rate of correlated pairs and double-pairs directly generated from the SFWM process. The total transmission and detection probability in each channel $k \in \{1, 2, 3, 4\}$, which includes transmission of the collection and filtering setup, splitting efficiency of the fiber based 50:50 beamsplitter and quantum efficiency of the detector in the respective channel is denoted by η_k. The optical losses in each channel are determined by measuring the transmission of a laser beam (at the target wavelength) from outside the vacuum chamber to just before the detector in each channel. We measure transmissions of $\approx 11.5\%$ each for Ch1 and Ch2 and 12.5% each for Ch3 and Ch4, which include the contributions from the filter-Etalon and fiber beamsplitter. Including the quantum efficiencies of APDs in each channel (about 60-70% per APD), the measured efficiencies (η'_k) for each channel are 0.078, 0.083, 0.080, and 0.067 for channels 1,2,3 and 4 respectively. These values provide an estimate of the upper bound for effective efficiencies, as they do not account for absorption in the atomic ensemble or spatial mode mismatch between the photons and the collection optics.

Since we expect additional losses that are frequency specific to the Stokes and anti-Stokes modes, we define $\eta_i = \eta_s \eta'_i$ for $i \in \{1, 2\}$ and $\eta_j = \eta_{as} \eta'_j$ for $j \in \{3, 4\}$. We then use equations D2 and D1 to estimate η_s and η_{as}. We infer additional losses that are $1 - \eta_s = 19\%$ for channels in the Stokes arm and $1 - \eta_{as} = 8\%$ for the anti-Stokes channels, which we attribute to a combination of above mentioned factors. Taking into account these additional losses, the total efficiencies are $\eta_1 = 0.022$ and $\eta_2 = 0.023$ for channels 1 and 2 pertaining to the Stokes modes, and the total efficiencies are $\eta_3 = 0.025$ and $\eta_4 = 0.021$ for channels 3 and 4 of the anti-Stokes mode.

Appendix D: Generation Rates from Detection Rates

We infer the generation rates of pairs g_p and double-pairs g_q from the detected accidental-corrected rates of pairs, triplets and quadruplets by factoring in the channel losses as follows. c_q, the accidental-corrected quadruplet rate, is solely contributed to by generated double-pairs as well. There are four possible combinations by which the two Stokes photons reach Ch1 and Ch2 each and the two anti-Stokes photons reach Ch3 and Ch4 each. This gives,

$$c_q = 4 g_q \eta_1 \eta_2 \eta_3 \eta_4. \tag{D1}$$

Similarly, double-pair generations are the sole contributors to accidental-corrected triplet coincidences. A triplet between channels 1, 3 and 4 occurs from two possible combinations by which the two anti-Stokes photons reach one of Ch3 and Ch4 each (leading to the factor $2\eta_3\eta_4$) combined with the probability that at least one of the two Stokes photons reaches Ch1 (leading to the factor $1-(1-\eta_1)^2$ where $(1-\eta_1)^2$ is the probability that neither of the two Stokes photons reaches channel 1). Applying this to all combinations of triplet detections,

$$\begin{aligned} c_{123} &= 2 g_q \eta_1 \eta_2 (2 - \eta_3) \eta_3 \\ c_{124} &= 2 g_q \eta_1 \eta_2 (2 - \eta_4) \eta_4 \\ c_{134} &= 2 g_q \eta_3 \eta_4 (2 - \eta_1) \eta_1 \\ c_{234} &= 2 g_q \eta_3 \eta_4 (2 - \eta_2) \eta_2. \end{aligned} \tag{D2}$$

We use this to estimate mean values of g_q. Since we have non-number-resolving detectors, both pairs and double-pairs from the SFWM process contribute to pair coincidence detections. A coincidence between channels 1 and 3 can be caused by a generated pair where the Stokes photon is detected in Ch1 and the anti-Stokes is detected in Ch3 ($\eta_1\eta_3$) or the probability that at least one of two Stokes and two anti-Stokes photons from a double-pair reach Ch1 and Ch3 respectively $((1-(1-\eta_1)^2)(1-(1-\eta_3)^2) = \eta_1\eta_3(2-\eta_1)(2-\eta_3))$. This gives,

$$\begin{aligned} c_{13} &= \eta_1 \eta_3 (g_p + g_q (2 - \eta_1)(2 - \eta_3)) \\ c_{14} &= \eta_1 \eta_4 (g_p + g_q (2 - \eta_1)(2 - \eta_4)) \\ c_{23} &= \eta_2 \eta_3 (g_p + g_q (2 - \eta_2)(2 - \eta_3)) \\ c_{24} &= \eta_2 \eta_4 (g_p + g_q (2 - \eta_2)(2 - \eta_4)) \end{aligned} \tag{D3}$$

where c_{ij} is the accidental-corrected pair rate between channels i and j.

We use measured accidental-corrected pair, triplet and quadruplet rates to obtain values for g_p and g_q, and the mean values are reported in section III E.

Appendix E: Accidental Correction Procedure

Correction must be performed to eliminate contributions from accidental coincidences between uncorrelated events from different channels. This can be visualized as the relative probability of two independent events falling within the same coincidence time window t_c (i.e. random chance), yielding the accidental rate $t_c R_i R_j$ for singles rates R_i and R_j in channels i and j. Excess coincidence events after correction can then only be attributed to actual correlations between channels: in the case of two channels i and j with an observed pair

rate of R_{ij}, the correlated pair rate c_{12} is given by

$$c_{ij} = R_{ij} - t_c R_i R_j.$$

The total correlated pair rate is $c_p = \sum_{i,j} c_{ij}$ for $\{i,j\} \in \{\{1,3\},\{1,4\},\{2,3\},\{2,4\}\}$.

These correlated pairs (and separately, accidentals) can be modeled as a separate stream of events that factor into the calculation of higher-order accidentals, e.g. 3-fold accidentals between channels i,j and k occur due to accidental coincidences across the individual channels $\{R_i, R_j, R_k\}$, as well as pairs with the remaining channel $\{c_{ij}, R_k\}$, $\{c_{ik}, R_j\}$ and $\{c_{jk}, R_i\}$. For instance, in Fig. 3) these correspond to the general background horizontal, vertical ridges and diagonal ridges when $\{i,j,k\} = \{s,3,4\}$.

The correlated triplet rate is thus

$$c_{ijk} = R_{ijk} - t_c\left(c_{ij}R_k + c_{jk}R_i + c_{ik}R_j\right) - t_c^2 R_i R_j R_k$$

given an observed triplet rate of R_{ijk}.

It can be seen that each of the individual terms contributing to the n-fold coincidences correspond to a possible partitioning of the set of all channels, with the total number of partitions given by Bell's number B_n (i.e. $B_2 = 2$, $B_3 = 5$, $B_4 = 15$). We write out explicitly the exhaustive 14-term correction performed for 4-fold coincidences,

$$\begin{aligned} c_{1234} = {} & R_{1234} \\ & - t_c\left(c_{12}c_{34} + c_{13}c_{24} + c_{14}c_{23}\right) \\ & - t_c\left(c_{123}R_4 + c_{124}R_3 + c_{134}R_2 + c_{234}R_1\right) \\ & - t_c^2\left(c_{12}R_3R_4 + c_{13}R_2R_4 + c_{14}R_2R_3\right) \\ & - t_c^2\left(c_{23}R_1R_4 + c_{24}R_1R_3 + c_{34}R_1R_2\right) \\ & - t_c^3 R_1R_2R_3R_4. \end{aligned}$$

We also make a small note that this correction slightly overestimates the actual accidental rate [45] due to the n-fold coincidence calculation method containing an implicit ordering of events that introduces excess accidentals. This overcompensation is minimized by using a small 20 ns coincidence window, yielding a raw quadruplet rate of 20.5 cps and lower bound correlated quadruplet rate of 3 cps with the experimental settings... Most of the accidentals are dominated by pair-pair accidentals (5.5 cps), followed by pair-acc-acc (5.6 cps) and triplet-acc (4.8 cps). **These numbers need to be updated based on actual calculations**

Code for the accidental correction as well as the corresponding datasets can be found in...

[1] J.-W. Pan, Z.-B. Chen, C.-Y. Lu, H. Weinfurter, A. Zeilinger, and M. Żukowski, Multiphoton entanglement and interferometry, Rev. Mod. Phys. **84**, 777 (2012).

[2] Z. Zhao, T. Yang, Y.-A. Chen, A.-N. Zhang, M. Żukowski, and J.-W. Pan, Experimental violation of local realism by four-photon greenberger-horne-zeilinger entanglement, Phys. Rev. Lett. **91**, 180401 (2003).

[3] H. Mikami, Y. Li, K. Fukuoka, and T. Kobayashi, New high-efficiency source of a three-photon w state and its full characterization using quantum state tomography, Phys. Rev. Lett. **95**, 150404 (2005).

[4] W. Dür, G. Vidal, and J. I. Cirac, Three qubits can be entangled in two inequivalent ways, Phys. Rev. A **62**, 062314 (2000).

[5] M. Hillery, V. Bužek, and A. Berthiaume, Quantum secret sharing, Phys. Rev. A **59**, 1829 (1999).

[6] Y.-A. Chen, A.-N. Zhang, Z. Zhao, X.-Q. Zhou, C.-Y. Lu, C.-Z. Peng, T. Yang, and J.-W. Pan, Experimental quantum secret sharing and third-man quantum cryptography, Phys. Rev. Lett. **95**, 200502 (2005).

[7] M. Mitchell, J. Lundeen, and A. Steinberg, Super-resolving phase measurements with a multiphoton entangled state, Nature **429**, 161 (2004).

[8] R. Raussendorf and H. J. Briegel, A one-way quantum computer, Phys. Rev. Lett. **86**, 5188 (2001).

[9] D. E. Browne and T. Rudolph, Resource-efficient linear optical quantum computation, Phys. Rev. Lett. **95**, 010501 (2005).

[10] M. Bourennane, M. Eibl, S. Gaertner, C. Kurtsiefer, A. Cabello, and H. Weinfurter, Decoherence-free quantum information processing with four-photon entangled states, Phys. Rev. Lett. **92**, 107901 (2004).

[11] M. ZUKOWSKI, A. ZEILINGER, and H. WEINFURTER, Entangling photons radiated by independent pulsed sources, Annals of the New York Academy of Sciences **755**, 91 (1995), https://nyaspubs.onlinelibrary.wiley.com/doi/pdf/10.1111/j.1749-6632.1995.tb38959.x.

[12] D. Bouwmeester, J.-W. Pan, M. Daniell, H. Weinfurter, and A. Zeilinger, Observation of three-photon greenberger-horne-zeilinger entanglement, Phys. Rev. Lett. **82**, 1345 (1999).

[13] H. Mikami, Y. Li, and T. Kobayashi, Generation of the four-photon w state and other multiphoton entangled states using parametric down-conversion, Phys. Rev. A **70**, 052308 (2004).

[14] Y. Li and T. Kobayashi, Four-photon w state using two-crystal geometry parametric down-conversion, Phys. Rev. A **70**, 014301 (2004).

[15] H.-S. Zhong, Y. Li, W. Li, L.-C. Peng, Z.-E. Su, Y. Hu, Y.-M. He, X. Ding, W. Zhang, H. Li, L. Zhang, Z. Wang, L. You, X.-L. Wang, X. Jiang, L. Li, Y.-A. Chen, N.-L. Liu, C.-Y. Lu, and J.-W. Pan, 12-photon entanglement and scalable scattershot boson sampling with optimal entangled-photon pairs from parametric down-conversion, Phys. Rev. Lett. **121**, 250505 (2018).

[16] A. Lamas-Linares, J. Howell, and D. Bouwmeester, Stimulated emission of polarization-entangled photons, Nature **412**, 887 (2001).

[17] C. Simon and D. Bouwmeester, Theory of an

entanglement laser, Phys. Rev. Lett. **91**, 053601 (2003).
[18] J. Tiedau, T. J. Bartley, G. Harder, A. E. Lita, S. W. Nam, T. Gerrits, and C. Silberhorn, Scalability of parametric down-conversion for generating higher-order fock states, Phys. Rev. A **100**, 041802 (2019).
[19] L.-b. Deng, L.-z. Zhang, and S.-g. Sun, Generalized two-mode squeezed states: Non-classical properties, Journal of Modern Optics **40**, 169 (1993).
[20] H. Weinfurter and M. Żukowski, Four-photon entanglement from down-conversion, Phys. Rev. A **64**, 010102 (2001).
[21] M. Eibl, S. Gaertner, M. Bourennane, C. Kurtsiefer, M. Żukowski, and H. Weinfurter, Experimental observation of four-photon entanglement from parametric down-conversion, Phys. Rev. Lett. **90**, 200403 (2003).
[22] N. Kiesel, M. Bourennane, C. Kurtsiefer, H. Weinfurter, D. Kaszlikowski, W. Laskowski, and M. Z. and, Three-photon w-state, Journal of Modern Optics **50**, 1131 (2003), https://www.tandfonline.com/doi/pdf/10.1080/09500340308234597.
[23] S. Bettelli, Comment on "Coherence measures for heralded single-photon sources", Physical Review A **81**, 037801 (2010).
[24] M. Razavi, I. Söllner, E. Bocquillon, C. Couteau, R. Laflamme, and G. Weihs, Characterizing heralded single-photon sources with imperfect measurement devices, Journal of Physics B: Atomic, Molecular and Optical Physics **42**, 114013 (2009).
[25] J.-M. Chen, C.-Y. Hsu, W.-K. Huang, S.-S. Hsiao, F.-C. Huang, Y.-H. Chen, C.-S. Chuu, Y.-C. Chen, Y.-F. Chen, and I. A. Yu, Room-temperature biphoton source with a spectral brightness near the ultimate limit, Phys. Rev. Res. **4**, 023132 (2022).
[26] S. Du, P. Kolchin, C. Belthangady, G. Y. Yin, and S. E. Harris, Subnatural linewidth biphotons with controllable temporal length, Physical Review Letters **100**, 183603 (2008).
[27] S. Du, J. Wen, and M. H. Rubin, Narrowband biphoton generation near atomic resonance, J. Opt. Soc. Am. B **25**, C98 (2008).
[28] P. Kolchin, Electromagnetically-induced-transparency-based paired photon generation, Physical Review A **75**, 033814 (2007).
[29] B. Srivathsan, G. K. Gulati, C. M. Y. Brenda, G. Maslennikov, D. Matsukevich, and C. Kurtsiefer, Narrow band source of transform-limited photon pairs via four-wave mixing in a cold atomic ensemble, Physical Review Letters **111**, 123602 (2013).
[30] V. Balić, D. A. Braje, P. Kolchin, G. Y. Yin, and S. E. Harris, Generation of paired photons with controllable waveforms, Physical Review Letters **94**, 183601 (2005).
[31] U. Leonhardt, Quantum physics of simple optical instruments, Reports on Progress in Physics **66**, 1207 (2003).
[32] A. I. Lvovsky, Squeezed light, in *Photonics* (John Wiley & Sons, Ltd, 2015) Chap. 5, pp. 121–163.
[33] N. Sangouard, C. Simon, H. De Riedmatten, and N. Gisin, Quantum repeaters based on atomic ensembles and linear optics, Reviews of Modern Physics **83**, 33 (2011).
[34] J. Wen and M. H. Rubin, Transverse effects in paired-photon generation via an electromagnetically induced transparency medium. i. perturbation theory, Physical Review A **74**, 023808 (2006).
[35] H. de Riedmatten, V. Scarani, I. Marcikic, A. Acin, W. Tittel, H. Zbinden, and N. Gisin, Two independent photon pairs versus four-photon entangled states in parametric down conversion, Journal of Modern Optics **51**, 1637 (2004), quant-ph/0310167.
[36] M.-X. Dong, W. Zhang, Z.-B. Hou, Y.-C. Yu, S. Shi, D.-S. Ding, and B.-S. Shi, Experimental realization of narrowband four-photon greenberger–horne–zeilinger state in a single cold atomic ensemble, Optics Letters **42**, 4691 (2017).
[37] J. Park and H. S. Moon, Generation of a bright four-photon entangled state from a warm atomic ensemble via inherent polarization entanglement, Applied Physics Letters **120**, 024001 (2022).
[38] Y. Wu, L. Tian, Z. Xu, W. Ge, L. Chen, S. Li, H. Yuan, Y. Wen, H. Wang, C. Xie, and K. Peng, Simultaneous generation of two spin-wave–photon entangled states in an atomic ensemble, Phys. Rev. A **93**, 052327 (2016).
[39] H. Hübel, D. R. Hamel, A. Fedrizzi, S. Ramelow, K. J. Resch, and T. Jennewein, Direct generation of photon triplets using cascaded photon-pair sources, Nature **466**, 601 (2010).
[40] Y. Jiang, Y. Mei, and S. Du, Quantum langevin theory for two coupled phase-conjugated electromagnetic waves, Physical Review A **107**, 053703 (2023).
[41] C. H. Raymond Ooi, Q. Sun, M. S. Zubairy, and M. O. Scully, Correlation of photon pairs from the double raman amplifier: Generalized analytical quantum langevin theory, Physical Review A **75**, 013820 (2007).
[42] P. Kolchin, S. Du, C. Belthangady, G. Y. Yin, and S. E. Harris, Generation of narrow-bandwidth paired photons: Use of a single driving laser, Physical Review Letters **97**, 113602 (2006).
[43] R. J. Glauber, The Quantum Theory of Optical Coherence, Physical Review **130**, 2529 (1963).
[44] J. H. Shapiro and K.-X. Sun, Semiclassical versus quantum behavior in fourth-order interference, Journal of the Optical Society of America B **11**, 1130 (1994).
[45] L. Jánossy, Rate of n-fold accidental coincidences, Nature **153**, 165 (1944).